

# An investigation on non-isothermal crystallization behavior and morphology of polyamide 6/ poly(ethylene-co-1-butene)-graft-maleic anhydride/organoclay nanocomposites

Sepideh Gomari, Ismaeil Ghasemi\*, Mohammad Karrabi, Hamed Azizi

Plastic Department, Iran Polymer and Petrochemical Institute, P.O.Box: 14965/115, Tehran, Iran.

Received: 26 January 2015, Accepted: 10 May 2015

## ABSTRACT

Nanocomposites based on polyamide 6 (PA6) and poly(ethylene-co-1-butene)-graft-maleic anhydride (EB-g-MAH) blends have been prepared via melt mixing. The effect of blend ratio and organoclay concentration on the crystallization and melting behavior of specimens were studied. Three types of commercial organo-modified clay (Cloisite 30B, Cloisite 15A and Cloisite 20A) were employed to assess the importance of the nanoclay polarity and gallery distance. The crystallization behavior was investigated using differential scanning calorimetry (DSC) and wide angle X-ray diffraction spectroscopy (WAXD). The strong interactions between amine end groups of PA6 and maleic anhydride groups of EB-g-MAH led to complete inhibition of EB-g-MAH crystallization according to the DSC results. A transformation from the  $\alpha$  form to the  $\gamma$  form crystals of PA6, induced by both organoclays and EB-g-MAH, was monitored by WAXD and DSC. Small angle X-ray scattering (SAXS) was used to evaluate the morphology of nanocomposites. Moreover, transmission electron microscopy (TEM) was conducted to determine the location of organoclays and indicated that the organoclays mainly present in the PA6 matrix and rarely distribute in the EB-g-MAH phase in the case of low polarity organoclays. It was also evidenced that the organoclay with the most affinity to PA6 (Cloisite 30B) had the largest effect on the thermal and crystallization behavior of this phase in the blend. **Polyolefins J (2015) 2: 99-108**

**Keywords:** polyamide 6; polyolefin elastomer; organoclay; crystallization; morphology

## INTRODUCTION

Polyamide 6 (PA6) is a semi-crystalline thermoplastic with great properties and many engineering applications. Since a disadvantage of PA6 is its low notched impact strength at sub-zero temperatures, melt blending with functionalized elastomers is an effective way to improve the toughness of PA6 [1, 2]. Polyolefin elastomers (POEs) which are a copolymer of ethylene and another  $\alpha$ -olefin such as butene or octene are

recently introduced as a new class of elastomers and can be used as a good impact modifier [3, 4]. POEs provide better efficiency of impact modification than ethylene-propylene rubber (EPR) and ethylene-propylene-diene rubber (EPDM) which are the most versatile commodity impact modifiers. By blending PA6 with a maleated polyolefin elastomer, the maleic anhydride groups of POE-g-MAH can react with the amine end groups of PA6 and make a graft copolymer, PA6-g-POE, which acts as a compatibilizer and enhances

\* Corresponding Author - E-mail: i.ghasemi@ippi.ac.ir

the interfacial adhesion between two phases [4, 5]. Whereas incorporating a low modulus material reduces the stiffness of polyamide 6, the addition of rigid filler particles, such as nanoclays, will give a good balance of toughness and stiffness [6, 7]. Nanoclays have a large aspect ratio and can display advanced properties even at very low loadings, whereas hydrophilic nature of these materials makes them low compatible with hydrophobic organic polymers. Thus for enhancing the compatibility and producing nanocomposites with favored morphologies, the interlayer cations of silicate layers are replaced with organic ammonium or phosphonium cations to make organoclays.

The crystalline structure and the degree of crystallinity of polyamide 6 are very important and have a profound influence on the final properties of the blend. PA6 can exist in either of two stable crystalline phases structures;  $\alpha$  and  $\gamma$  forms. The  $\alpha$  form is consisted of chains which are in the fully extended planar zig-zag conformation. In this structural mode, hydrogen bonds form between anti-parallel chains, whereas in the  $\gamma$  form the amide groups tilt with respect to the chain axis and the parallel chains are joined to each other by hydrogen bonds [8]. These conformations give rise to a lesser thermodynamic stability in the  $\gamma$  form compared to the  $\alpha$  form. It is well known that the crystallization behavior of polymer matrix is affected by the presence of a second component (e.g., elastomer or rigid fillers). A large number of researchers [9-11] implied a transition of the crystal structure of PA6 from  $\alpha$  to  $\gamma$  form after incorporation of organoclay. As suggested by Liu and Wu [12], the main reason for development of  $\gamma$  form crystals of PA6 is ionically bonded protonated amino end groups of polyamide chains on the negatively charged silicate layers which serve as the nucleation sites. Wu and Liao [13] have investigated the structural change of PA6/clay nanocomposites prepared by in-situ polymerization and found that the layered saponite may increase the crystallization rate of the  $\alpha$  form crystals at low contents, while in the higher contents it can promote the heterogeneous nucleation of  $\gamma$  form crystals. Cui and Yeh [14] observed the crystal phase transition of  $\gamma$  to  $\alpha$  form crystals of PA6 by increasing the poly (vinyl alcohol) (PVA) content in the PA6/PVA nanocomposites, because the clay platelets has gradually migrated into the PVA phase. Chiu et al. [15] studied the crystal forms of PA6 in its blend with a maleic anhydride grafted polyolefin elastomer at

the presence of organically modified nanoclay. They realized that the addition of elastomeric phase and/or organoclay developed the formation of  $\gamma$  form crystals. Furthermore, a faster cooling rate increased the formation of  $\gamma$  crystals indicating that they were kinetically more favorable than  $\alpha$  form crystals.

Specific interactions between polymer matrix and organoclay, e.g., hydrogen bonding, dipole-dipole interaction, ionic interaction, etc, provide more compatibility of these pairs. As described by Lee and Han [16] the degree of compatibility between polymer chains and organoclay determines the degree of dispersion of organoclay platelets, which in turn dominates the crystallization and melting behavior of polymer matrix. The structure of organo-modifier which is applied in the nanoclay platelets governs the degree of interaction and compatibility of polymer matrix and nanoclay. To our knowledge, the influence of organoclay modifier on the melting behavior and the crystal forms of toughened PA6 has not been studied sufficiently. The main objective of this study is to investigate the effect of organoclay type on the crystallization behavior and thermal properties of PA6/poly(ethylene-co-1-butene)-graft-maleic anhydride/organoclay nanocomposites using DSC and WAXD. The effect of blend ratio and organoclay concentration has been also discussed. Since the distribution and morphology of nanoclay has an important role in crystallization behavior of the compound, the location and morphology of nanoclay was tracked using TEM and SAXS.

## EXPERIMENTAL

### Material

PA6 with trade name of Akulon F-223D and density of 1.13 g/cm<sup>3</sup> was obtained from DSM, Netherlands, and dried in a vacuum oven at 80°C for 24 h prior to melt mixing. Poly(ethylene-co-1-butene) grafted with 0.5% maleic anhydride (EB-g-MAH) consisted of 67.9% ethylene and 31.6% butene (TAFMER MH7010) manufactured by Mitsui Chemicals, Inc., Japan, was used as polyolefin elastomer. Three different types of commercial organoclay used in this study including Cloisite 15A, Cloisite 20A and Cloisite 30B, were purchased from Southern Clay Products, USA. Characteristics of these organoclays and the structure of alkyl ammonium ions used for their modification

are listed in Table 1. Functionality, packing density, and length of these modifiers, are important parameters which determine the compatibility of organoclay with a given polymer [17]. The presence of hydroxyl groups in the modifier of Cloisite 30B makes it more compatible with polar polymers. The modifiers of Cloisite 15A and Cloisite 20A are the same but with different concentrations which increases d-spacing for Cloisite 15A. Organoclays were also dried in the same condition as PA6 before using.

### Sample preparation

The polymeric materials were dry-blended and then added to the mixing chamber of a Brabender internal mixer, Germany, with roller type rotors at temperature of 230°C and rotor speed of 60rpm. Organoclay was added after 2.5 min and mixing continued up to 10 min. Blend composition selected as 90/10, 80/20 and 70/30 (w/w) of PA6/EB-g-MAH and organoclay concentration selected as 0, 2 and 5 phr. Formulation and notation of the samples are reported in Table 2.

### Characterization

The crystallization and melting behavior of the samples were studied using a NETZSCH-200F3 Maia DSC, Germany. At the first step, the samples were heated to 250°C and kept for 5 minutes to eliminate their thermal history and then cooled to the room temperature at the rate of 10°C/min. Subsequently, the specimens were heated at the same rate to 250°C in order to investigate the corresponding melting behavior. Degree of crystallinity ( $X_c$ ) of specimens

were calculated using the following equation:

$$X_c = \frac{\Delta H_f}{w \times \Delta H_f^\circ} \times 100 \quad (1)$$

Where  $w$  is the weight fraction of PA6 in the sample and  $\Delta H_f$  and  $\Delta H_f^\circ$  are the heat of fusion of PA6 in the specimen and PA6 with 100% crystallinity, respectively.  $\Delta H_f^\circ$  was 190 J/g [18].

WAXD analyses were performed for the neat blend and different nanocomposites on a Siemens D5000, Germany, at 35 kV and 20 mA, using Cu K $\alpha$  radiation source ( $\lambda = 0.154$  nm) at  $2\theta$  range from 13-30°.

To evaluate the morphology of nanocomposites, SAXS and TEM were used. SAXS patterns were obtained on Hecus S3-MICROpix using Cu K $\alpha$  radiation source ( $\lambda = 0.154$  nm) operated at 50 kV and 40 mA. The scanning rate was 1°/min. TEM observations were conducted on a Philips EM2085, Netherlands, using an accelerating voltage of 100 kV. Ultrathin sections of the nanocomposite samples with a thickness of about 100 nm were cryo-microtomed by a Reichert OMU3 ultramicrotome, Austria, from the middle part of compression molded sheets of the samples (prepared in 240°C and 10 MPa using a press machine, Toyoseiki, Japan).

## RESULTS AND DISCUSSION

In order to get better insight into the morphology and location of organoclays in the PA6/EB-g-MAH

**Table 1.** Typical properties of the used organoclays.

Organoclay	Modifier structure	Modifier concentration (meq/100g clay)	d-spacing (nm)
Cloisite 30B	$\begin{array}{c} \text{CH}_2\text{CH}_2\text{OH} \\   \\ \text{CH}_3 - \text{N}^+ - \text{T} \\   \\ \text{CH}_2\text{CH}_2\text{OH} \end{array}$	90	1.85
Cloisite 20A	$\begin{array}{c} \text{CH}_3 \\   \\ \text{CH}_3 - \text{N}^+ - \text{HT} \\   \\ \text{HT} \end{array}$	95	2.42
Cloisite 15A	$\begin{array}{c} \text{CH}_3 \\   \\ \text{CH}_3 - \text{N}^+ - \text{HT} \\   \\ \text{HT} \end{array}$	125	3.15

HT is hydrogenated tallow (~65% C18; ~30% C16; ~5% C14).

**Table 2.** Samples formulation and notation.

Sample name	Composition	PA6/EB-g-MAH (w/w)	Organoclay concentration (phr <sup>(a)</sup> )
PA70-EB30	PA6/EB-g-MAH	70/30	0
PA70-20A2	PA6/EB-g-MAH/ Cloisite 20A	70/30	2
PA70-20A5	PA6/EB-g-MAH/ Cloisite 20A	70/30	5
PA70-30B2	PA6/EB-g-MAH/ Cloisite 30B	70/30	2
PA70-15A2	PA6/EB-g-MAH/ Cloisite 15A	70/30	2
PA80-20A2	PA6/EB-g-MAH/ Cloisite 20A	80/20	2
PA90-20A2	PA6/EB-g-MAH/Cloisite 20A	90/10	2

<sup>(a)</sup> phr is the abbreviation of parts per hundred parts of resin.

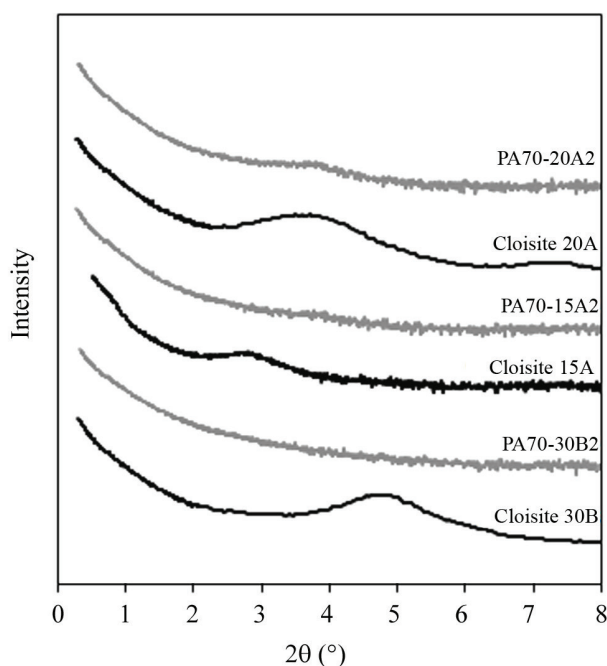
(70/30 w/w) blends, SAXS and TEM analysis were employed. Figure 1 shows the SAXS patterns of nanocomposites and neat organoclays. As can be seen, the characteristic peak of organoclay in the nanocomposites containing Cloisite 30B and 15A has been completely disappeared, so that the morphology of these samples is characterized by existence of individual silicate platelets and this grants the formation of a fully exfoliated structure. However, the nanocomposite including Cloisite 20A exhibited a peak at  $2\theta=3.7^\circ$ , the same  $2\theta$  as characteristic peak of neat organoclay, but with a reduced intensity. It can be concluded that this nanoclay has predominantly gained an intercalated morphology. For Cloisite 30B the existence of a strong interaction and high degree of hydrogen bonding between OH groups of organoclay modifier and amine end groups of PA chains could be responsible for good exfoliation of organoclay layers

[19, 20]. As mentioned earlier, Cloisite 15A and 20A have the same modifier and thus similar interactions with polyamide chains, but the former has a larger gallery distance. This would promote an easier penetration of polymeric chains into the interlayer of organoclay platelets and makes a better dispersion of Cloisite 15A in the polymer matrix.

TEM micrographs of the nanocomposites containing 2 phr of different organoclays have shown in Figure 2. The light areas are corresponded to EB-g-MAH phase and dark lines are referred to organoclay platelets. Figure 2-a reveals the complete exfoliation of Cloisite 30B. Furthermore, it can be seen that organoclay platelets are fully distributed in PA6 phase which implies high affinity of this nanoclay into the polar polyamide. For the sample containing Cloisite 15A (Figure 2-b) an exfoliated structure and for the sample with Cloisite 20A (Figure 2-c) an intercalated morphology can be detected which are in agreement with SAXS results. As reported in our previous paper [20], both of these organoclays are mainly presented in PA6, but a few part of clay particles are discerned in the EB-g-MAH domains (indicated by arrows).

It is expected that the crystallization behavior of PA6 phase in the blend is affected by the presence of organoclay. Figure 3-a shows the cooling scan of DSC thermograms of the neat PA6, EB-g-MAH, their blend (70/30 w/w) and the nanocomposites at different concentrations of Cloisite 20A. The EB-g-MAH curve shows an exothermic peak at  $38.2^\circ\text{C}$  ( $T_c$ ), representing a crystalline region, while no crystallization peak was observed for EB-g-MAH in the blend and nanocomposites. It seems that the strong interactions between maleic anhydride groups of EB-g-MAH and amine end groups of PA6 completely inhibited the crystallization of this phase.

The crystallization temperature value for pure PA6 ( $T_c=166.7^\circ\text{C}$ ) has shifted toward higher values ( $T_c=188.7^\circ\text{C}$ ) by addition of 30 wt% of EB-g-MAH

**Figure 1.** SAXS patterns of neat organoclays and nanocomposites.

which is an indication of a faster crystallization. This is similar to the results found by Ying et al. [21], where the crystallization behavior of PP/POE blends was investigated and showed that at low contents of polyolefin elastomer, the heterogeneous nucleation of POE accelerated the nucleation of PP during

crystallization. After incorporation of organoclay, a further increase in the  $T_c$  of PA6 has been detected. This could be attributed to the nucleation effect of organoclay platelets which were located in PA6 phase. As Benderly et al. [22] discussed, the nucleation effect of inorganic filler particles for PA6 in an immiscible blend is possible when the platelets are located in this phase. However, organoclays can decline the formation of crystals which decreases the intensity and area of crystallization peak. The enthalpies of crystallization ( $\Delta H_c$ ) of the samples are listed in Table 3.

On the second heating scan (see Figure 3-b) only one endothermic peak at 221°C was observed for neat PA6, which is ascribed to the melting of  $\alpha$  crystals and denoted as  $T_{m,\alpha}$ . By addition of elastomeric phase and organoclay, another endothermic peak was appeared around 214°C corresponding to  $\gamma$  crystals and defined as  $T_{m,\gamma}$ . The  $\gamma$  crystals always show lower melting temperature compared to the more stable  $\alpha$  crystals. It can be clearly seen that the neat PA6 only has  $\alpha$  crystals, while EB-g-MAH and organoclay have imposed the formation of  $\gamma$  crystals. Interestingly, the organoclay layers show higher potential to change the crystalline forms of PA6 in comparison to EB-g-MAH. With increase of the organoclay concentration (from 2 phr in the sample PA70-20A2 to 5 phr in the sample PA70-20A5), the values of enthalpy of fusion of higher melting endotherm,  $T_{m,\alpha}$ , slightly decreased while the values of lower melting endotherm,  $T_{m,\gamma}$ , enhanced. The quantitative values of enthalpy of fusion ( $\Delta H_f$ ) and degree of crystallinity ( $X_c$ ) are also

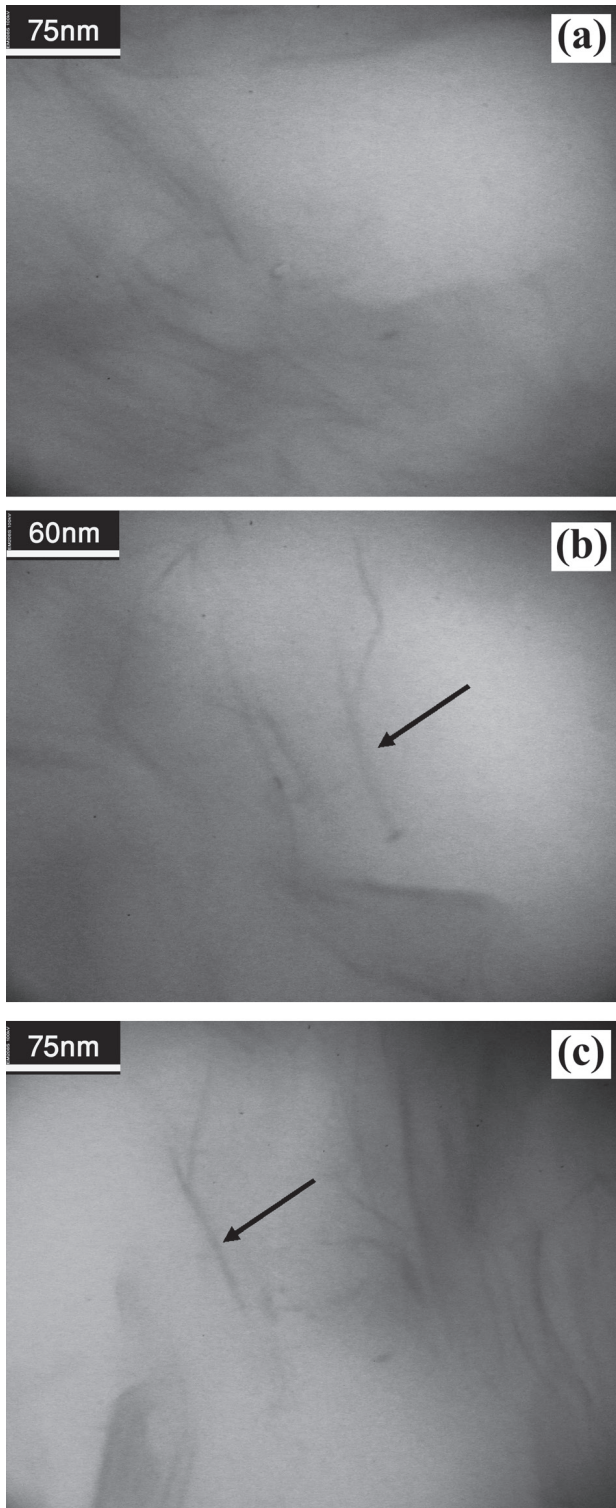


**Figure 2.** TEM micrographs of nanocomposites, PA70-30B2 (a), PA70-15A2 (b) and PA70-20A2 (c).

**Table 3.** DSC results for the samples, the effect of different parameters.

Samples	$\Delta H_c$ (J/g)	$\Delta H_f$ (J/g)	$X_c$ (%)
Effect of organoclay concentration			
PA70-EB30	47.70	50.54	38.00
PA70-20A2	44.48	46.48	35.65
PA70-20A5	41.16	43.72	34.52
Effect of blend composition			
PA90-20A2	58.60	61.97	36.96
PA80-20A2	49.52	53.88	36.16
PA70-20A2	44.48	46.48	35.65
Effect of organoclay type			
PA70-30B2	39.36	44.44	34.08
PA70-20A2	44.48	46.48	35.65
PA70-15A2	40.73	45.33	34.76

reported in Table 3.  $X_c$  was calculated from the DSC thermograms according to equation (1) and showed a reduction by increasing the organoclay content. This observation is similar to the results of previous studies [23-24].

The effect of blend composition on the crystallization and melting behavior of the nanocomposites containing 2 phr of organoclay (Cloisite 20A) is shown in Figure 4. In the cooling scan (Figure 4-a), no considerable change in the  $T_c$  is detected, however its magnitude and degree of crystallinity (as reported in Table 3) have decreased by reduction in the PA6 content. As mentioned earlier, most of nanoparticles are distributed in PA6 phase. Consequently, by decreasing the amount of PA6, the concentration of

organoclay in this phase has been enhanced, which can promote the inhibition effect of organoclay on the perfection of PA6 crystals. In addition, as examined by Wang et al. [25], increasing the content of EB-g-MAH had improved the probability of chemical reaction between the maleic anhydride groups of this polymer and amine end groups of PA6 to produce PA6-g-EB copolymers. The possible chemical reaction is presented in Wahit et al study [26]. These copolymers are able to disarrange the PA6 chains and thus reduce the degree of crystallinity.

In the heating curves in Figure 4-b, it was observed that by reducing the PA6 content, the magnitude of  $T_{m,\alpha}$  has been significantly decreased. For the samples containing higher amounts of PA6, a third peak in

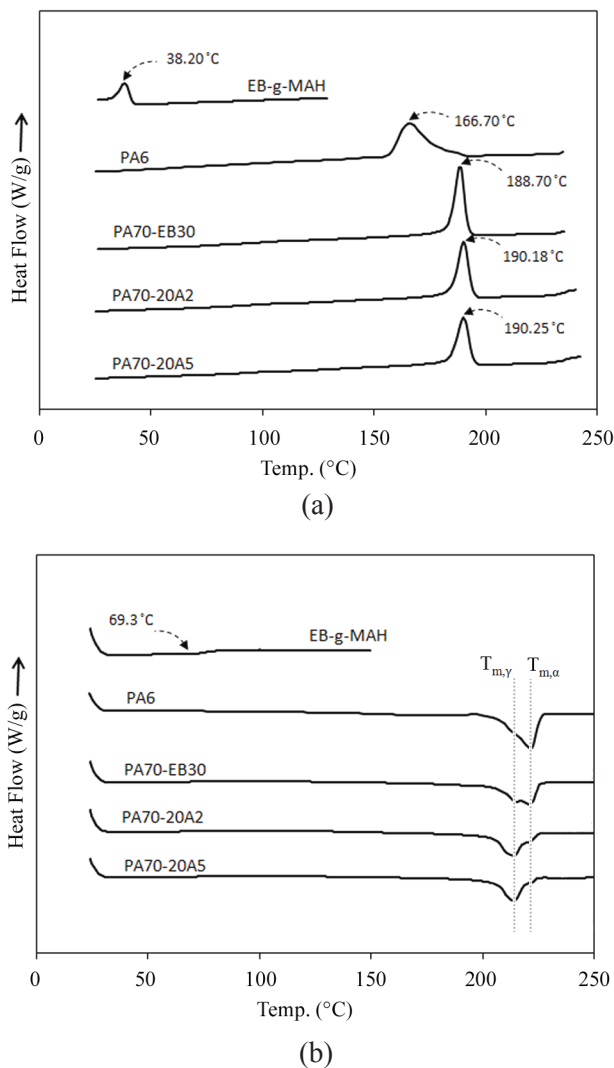


**Figure 3.** DSC thermograms of neat components, PA6/EB-g-MAH blend (70/30 w/w) without and with Cloisite 20A: The effect of organoclay concentration (a) cooling and (b) second heating scan.

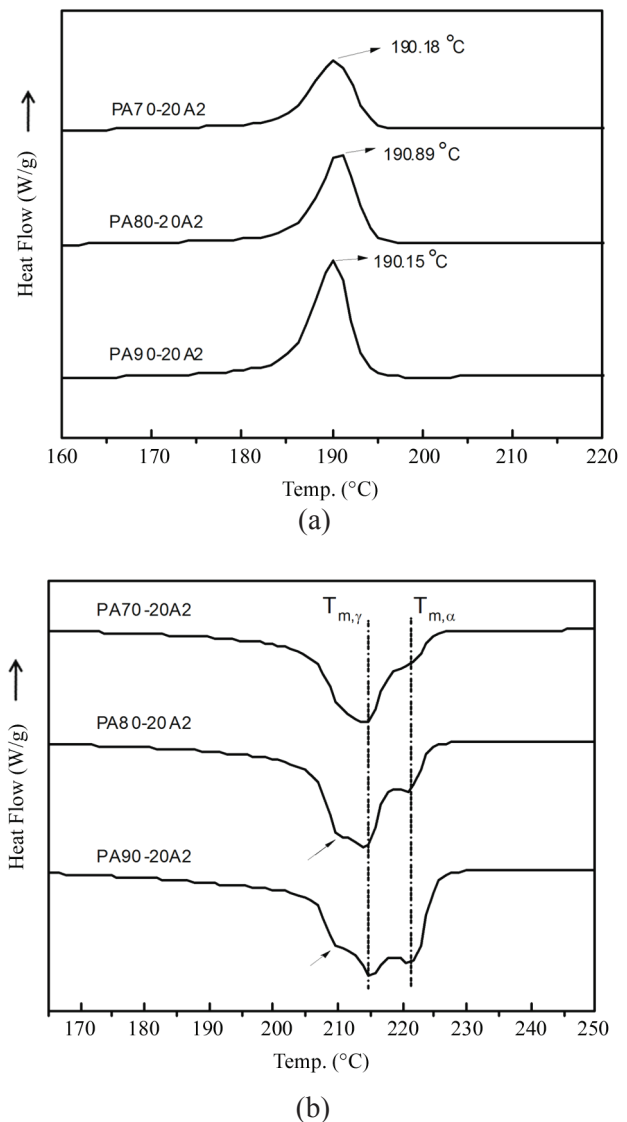


**Figure 4.** DSC thermograms of samples with 2 phr of Cloisite 20A: The effect of blend composition (a) cooling and (b) second heating scan.

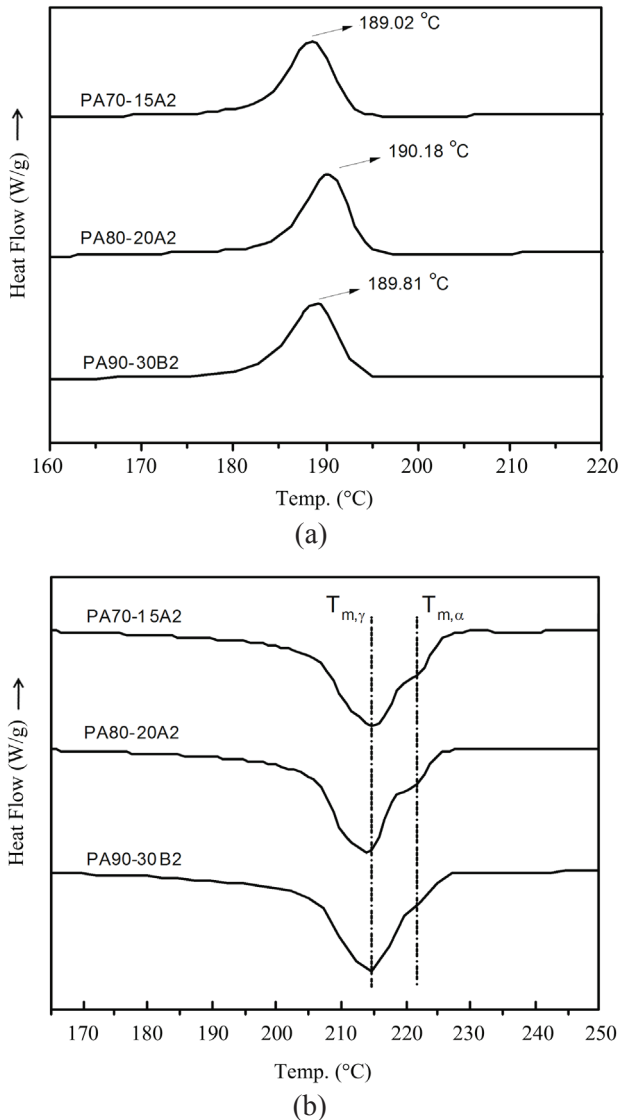


**Figure 5.** DSC thermograms of PA6/EB-g-MAH/organoclay nanocomposites: The effect of organoclay type (a) cooling and (b) second heating scan.

the left side of  $T_{m,\gamma}$  was appeared. This peak could be attributed to the melting of less stable  $\alpha$  form crystals which were transformed into the more stable  $\alpha$  form through the “melting-recrystallization-remelting” process as suggested by Chiu et al. [15]. In other words, during cooling step such less stable  $\alpha$  form crystals were formed and then during heating they would melt and recrystallize into more stable  $\alpha$  form crystals. This could also be an evidence for higher fraction of  $\alpha$  crystal in these samples.

Melting behavior of PA6 and its nanocomposite materials with various organoclays is presented in Figures 5-a and 5-b. The DSC thermograms during cooling step showed a sharp crystallization peak for all samples and the highest  $T_c$  was associated to the

sample containing Cloisite 20A.  $\Delta H_c$  and  $X_c$  of this sample, also showed higher values in respect to the two other organoclays (Table 3). As discussed in previous sections, Cloisite 20A has an intercalated morphology in the nanocomposite, whereas Cloisite 15A and Cloisite 30B are exfoliated. It seems that the exfoliation of organoclays would obstacle the perfect organization of polymeric chains which in turn reduces the degree of crystallinity and heat of crystallization. Furthermore, the intensity of interaction between organoclay and polyamide chains could be another effective parameter on the degree of crystallization, i.e., strong interactions would inhibit the arrangement of chains. In the heating scan (Figure 5-b) a mixed structure of  $\alpha$  and  $\gamma$  crystals was observed for PA6 in all the samples. The type of organoclay has no considerable influence on the crystal forms, because the magnitude of  $T_{m,\alpha}$  and  $T_{m,\gamma}$  were almost the same for three nanocomposites. According to Cervantes-Uc et al. analysis on the thermal degradation of commercially available organoclays, the onset temperature decomposition from TGA for Cloisite 20A, Cloisite 15A and Cloisite 30B is 198, 192 and 174°C, respectively [27]. However, the rate of surfactant loss increases dramatically in the range 240-400°C. Thus, a probable reason for the less impressive effect of organoclay type on degree of crystallinity and crystal structures may be attributed to possible decomposition of clay modifiers at processing temperature (230°C).

Wide angle X-ray diffraction patterns analyzed to gain insight about how the organoclay concentration, blend composition and organoclay type can affect the crystalline morphology of polyamide 6 in more detail. The diffraction peaks of the  $\alpha$  form crystals are located around  $2\theta=21^\circ$  and  $24^\circ$  which are corresponded to (200) and (002)/(202) planes, respectively. The characteristic peaks of (020), (001) and (200)/(201) planes of  $\gamma$  form crystals show up at  $2\theta=11^\circ$ ,  $22^\circ$  and  $23^\circ$ , respectively. The typical WAXD patterns of the samples in  $2\theta$  range of  $13-30^\circ$  are shown in Figure 6. As seen in Figure 6-a, only  $\alpha$  form crystal is detected for neat blend (sample PA70-EB30) while by addition of nanoclay the intensity of  $\alpha$  peaks decreased and diffraction peaks of  $\gamma$  form crystals was built up. However, regarding to DSC experiments, the  $\gamma$  form crystal was also distinguished in the sample PA70-EB30 (Figure 3-b).

All blend ratios containing 2 phr of Cloisite 20A showed both  $\alpha$  and  $\gamma$  form crystals with a higher  $\gamma$

form proportion, as depicted in Figure 6-b. This is in agreement with DSC results. Figure 6-c explains the formation of  $\gamma$  form crystallites for nanocomposites with different types of organoclay. The part of  $\gamma$  form crystals is more than  $\alpha$  forms for all samples. In the sample containing Cloisite 30B, the reduction

of intensity of crystal peaks compared to the other organoclays revealed that more interactions of this organoclay with PA6 chains had prevented the perfection of crystals, thus the degree of crystallinity was reduced. As observed by TEM, this organoclay was fully distributed in PA6 with an exfoliated morphology. Thus, it could alter the crystallization behavior of PA6 more than the two other organoclays.

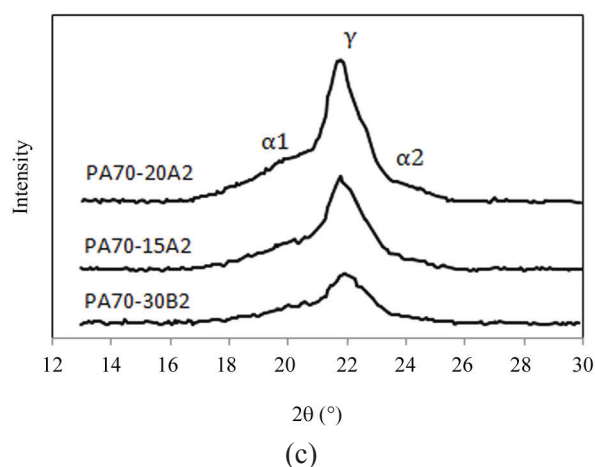
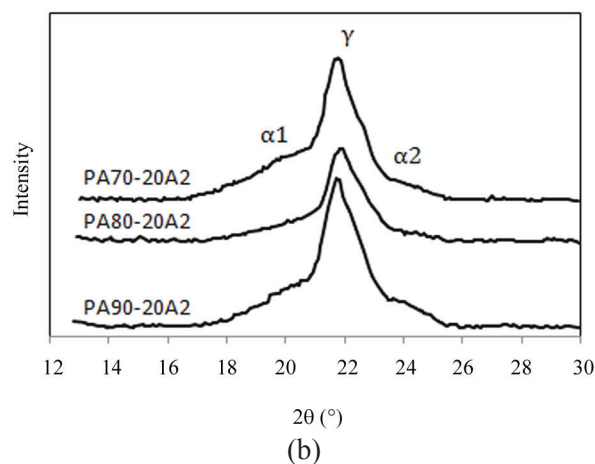
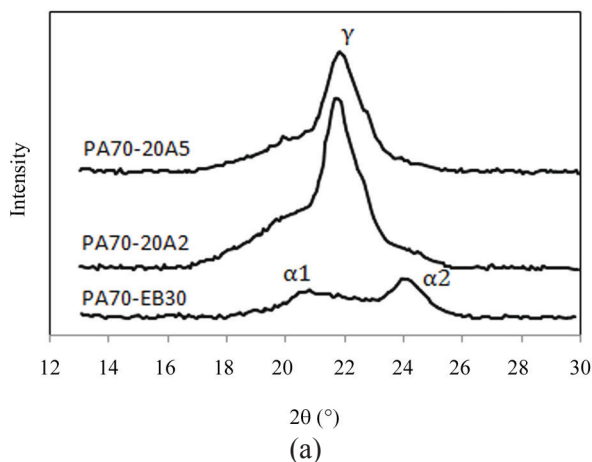


**Figure 6.** WAXD patterns of the samples: (a) The effect of organoclay concentration, (b) The effect of blend composition and (c) The effect of organoclay type.

## CONCLUSION

The nanocomposites based on toughened PA6 with a maleated polyolefin elastomer (EB-*g*-MAH) were prepared by an internal mixer with three different organoclay types. The effect of blend composition and organoclay content was also investigated. The nanocomposites morphology and degree of dispersion of organoclays were evaluated by SAXS. TEM observations were employed to confirm the nanocomposite morphology and determine the distribution and phase location of organoclays. It was concluded that Cloisite 30B which has a higher polarity compared to the other organoclays was fully distributed in PA6 phase with an exfoliated structure. This observation implies that there is strong affinity between Cloisite 30B and PA6 chains, due to interaction between amine groups of PA6 and OH groups in the modifier of this organoclay. However, Cloisite 15A and Cloisite 20A preferentially presented in the PA6 and rarely located in the elastomeric phase. An exfoliated morphology and an intercalated morphology were obtained for these two organoclays, respectively.

The thermal and crystallization behavior of samples were studied using DSC and WAXD measurements. The DSC thermograms of the blends and nanocomposites showed no crystallization peak for EB-*g*-MAH phase during cooling step which was probably related to the strong interactions of PA6 and EB-*g*-MAH. In the heating scans, a crystal form transition from  $\alpha$  to  $\gamma$  crystals of PA6 was detected after addition of both elastomeric phase and organoclay. However, the influence of organoclay was more considerable. The formation of  $\gamma$  crystals by addition of organoclay was also confirmed by WAXD analysis. The degrees of crystallinity were calculated based on the DSC results and revealed that the addition of organoclay significantly reduced  $X_c$  of the PA6. It was

obtained that the chemistry of organoclay modifier has an important role in the degree of dispersion of nanoclay, its localization and crystallization behavior of the polymer matrix. The organoclay with higher polarity and the exfoliated structure in the nanocomposite (Cloisite 30B) produced the lowest degree of crystallinity in comparison to the other organoclays.

## REFERENCES

- Gonzalez I, Eguiazabal J, Nazabal J (2005) Compatibilization level effects on the structure and mechanical properties of rubber modified polyamide 6/clay nanocomposites. *J Polym Sci B: Polym Phys* 43: 3611-3620
- Huang J, Keskkula H, Paul D (2006) Comparison of the toughening behavior of nylon 6 versus an amorphous polyamide using various maleated elastomers. *Polymer* 47: 639-651
- Chen X, Yu J, Luo Z, Guo S, He M, Zhou Z (2011) Study on mechanical properties and phase morphology of polypropylene/polyolefin elastomer/magnesium hydroxide ternary composites. *Polym Adv Technol* 22: 657-663
- Qiu G, Liu G, Qiu W, Liu S (2013) Phase morphology and mechanical properties of polyamide-6/ polyolefin elastomer- g - maleic anhydride blends. *J Macromol Sci, B* 53: 615-624
- Choi M, Jung J-Y, Chang Y-W (2014) Shape memory thermoplastic elastomer from maleated polyolefin elastomer and nylon 12 blends. *Polym Bull* 71: 625-635
- Nishitani Y, Yamada Y, Ishii C, Sekiguchi I, Kitano T (2010) Effects of addition of functionalized SEBS on rheological, mechanical, and tribological properties of polyamide 6 nanocomposites. *Polym Eng Sci* 50: 100-112
- Isik-gulsac I, Yilmazer U, Bayram G (2013) Effects of addition order of the components on polyamide-6/ organoclay/ elastomer ternary nanocomposites. *Adv Polym Technol* 32: E675-E691
- Kohan MI, Kohan MI (1995). *Nylon plastics handbook*, Hanser Publishers
- Lincoln DM, Vaia RA, Wang ZG, Hsiao BS (2001) Secondary structure and elevated temperature crystallite morphology of nylon-6/layered silicate nanocomposites. *Polymer* 42: 1621-1631
- Maiti P, Okamoto M (2003) Crystallization controlled by silicate surfaces in nylon 6 clay nanocomposites. *Macromol Mater Eng* 288: 440-445
- Li TC, Ma J, Wang M, Tjiu WC, Liu T, Huang W (2007) Effect of clay addition on the morphology and thermal behavior of polyamide 6. *J Appl Polym Sci* 103: 1191-1199
- Liu X, Wu Q (2002) Phase transition in nylon 6/ clay nanocomposites on annealing. *Polymer* 43: 1933-1936
- Wu TM, Liao CS (2000) Polymorphism in nylon 6/clay nanocomposites. *Macromol Chem Phys* 201: 2820-2825
- Cui L, Yeh JT (2010) Nylon 6 crystal phase transition in nylon 6/ clay/ poly (vinyl alcohol) nanocomposites. *J Appl Polym Sci* 118: 1683-1690
- Chiu FC, Lai SM, Chen YL, Lee TH (2005) Investigation on the polyamide 6/ organoclay nanocomposites with or without a maleated polyolefin elastomer as a toughener. *Polymer* 46: 11600-11609
- Lee KM, Han CD (2003) Rheology of organoclay nanocomposites: Effects of polymer matrix/ organoclay compatibility and the gallery distance of organoclay. *Macromolecules* 36: 7165-7178
- Xie W, Gao Z, Pan W-P, Hunter D, Singh A, Vaia R (2001) Thermal degradation chemistry of alkyl quaternary ammonium montmorillonite. *Chem Mater* 13: 2979-2990
- Brandrup J (1989) *Polymer Handbook*. 3rd ed. John Wiley and Sons, New York
- Paci M, Filippi S, Magagnini P (2010) Nanostructure development in nylon 6-Cloisite® 30B composites. Effects of the preparation conditions. *Eur Polym J* 46: 838-853
- Gomari S, Ghasemi I, Karrabi M, Azizi H (2012) Organoclay localization in polyamide 6/ethylene-butene copolymer grafted maleic anhydride blends: The effect of different types of organoclay. *J Polym Res* 19: 1-11
- Ying JR, Liu SP, Guo F, Zhou XP, Xie XL (2008) Non-isothermal crystallization and crystalline structure of PP/POE blends. *J Therm Anal Calorim* 91: 723-731
- Benderly D, Siegmans A, Narkis M (1997) Structure and behavior of multicomponent

- immiscible polymer blends. *J Polym Eng* 17: 461-490
23. Zhang L, Wan C, Zhang Y (2008) Polyamide 6/ maleated ethylene - propylene - diene rubber/ organoclay composites with or without glycidyl methacrylate as a compatibilizer. *J Appl Polym Sci* 110: 1870-1879
  24. Katoh Y, Okamoto M (2009) Crystallization controlled by layered silicates in nylon 6–clay nano-composite. *Polymer* 50: 4718-4726
  25. Wang B, Hao L, Wang W, Hu G (2009) One-step compatibilization of polyamide 6/poly (ethylene-1-octene) blends with maleic anhydride and peroxide. *J Polym Res* 17: 821-826
  26. Wahit M, Hassan A, Mohd Ishak Z, Czigány T (2009) Ethylene-octene copolymer (POE) toughened polyamide 6/ polypropylene nanocomposites: Effect of POE maleation. *Express Polym Lett* 3: 309-319
  27. Cervantes-Uc JM, Cauich-Rodríguez JV, Vázquez-Torres H, Garfias-Mesías LF, Paul DR (2007) Thermal degradation of commercially available organoclays studied by TGA–FTIR. *Thermochim Acta* 457: 92-102